Letters in High Energy Physics
ISSN: 2632-2714

Volume 2024
September

First-Principles Study of Dopant-Induced Structural, Electronic and Thermoelectric Properties of $RbSnX_3$ Perovskites

Lalnunpuia[1], Lalmuanawma Chhangte[2,*], T Malsawmtluanga[2], Lalrintluanga Sailo[3], Lawrence Zonunmawia[3], Remlalsiama[3], Zaithanzauva Pachuau[4], Malsawmtluanga[5]

[1]Department of Physics, Govt. Champhai College, Champhai, Mizoram, India

[2]Department of Physics, Lunglei Govt. College, Lunglei, Mizoram, India

[3]Department of Physics, Govt. Zirtiri Res. Sc. College, Aizawl, Mizoram, India

[4]Department of Physics, Mizoram University, Aizawl, Mizoram, India

[5]Research Scholar, Mizoram University, Aizawl, Mizoram, India

[*]Corresponding Author: muana.chhangte@gmail.com

Abstract:

This work reports a comprehensive first-principles investigation of the structural, electronic, and thermoelectric properties of $RbSnX_3$ (X = Cl, Br, I) halide perovskites. Structural stability is confirmed through formation energy and elastic criteria, satisfying mechanical stability conditions. Electronic structure calculations reveal direct bandgap semiconducting behavior, with bandgaps decreasing systematically from Cl to I due to enhanced orbital interactions. Thermoelectric properties are evaluated within the Boltzmann transport framework. The results indicate high Seebeck coefficients, moderate electrical conductivity, and low lattice thermal conductivity, which collectively enhance thermoelectric efficiency. The dimensionless figure of merit (ZT) exhibits significant improvement with increasing temperature, reaching optimal values at elevated conditions. Among the studied compounds, $RbSnI_3$ demonstrates superior performance due to its favorable carrier transport properties. These findings suggest that $RbSnX_3$ perovskites are promising lead-free candidates for thermoelectric energy conversion applications.

Keywords: Halide perovskites; First-principles calculations; Density functional theory; Thermoelectric properties; Seebeck coefficient.

1. Introduction

The rapid depletion of fossil fuel reserves and the escalating demand for sustainable energy technologies have intensified the search for efficient materials capable of energy conversion and harvesting. Among various approaches, thermoelectric (TE) materials have emerged as promising candidates due to their ability to directly convert waste heat into electrical energy, offering a solid-state and environmentally benign solution [1]. The efficiency of thermoelectric materials is governed by the dimensionless figure of merit (ZT), which depends on a delicate balance between Seebeck coefficient, electrical conductivity, and thermal conductivity. Achieving high ZT remains a fundamental challenge due to the interdependent nature of these parameters [2].

In recent years, halide perovskites with the general formula ABX_3 have attracted considerable attention owing to their remarkable optoelectronic and transport properties. In particular, lead-free inorganic perovskites have gained prominence as environmentally friendly alternatives to conventional Pb-based compounds, which suffer from toxicity and long-term instability issues [3]. Among these, $RbSnX_3$ (X = Cl, Br, I) perovskites exhibit favorable semiconducting behavior, tunable bandgaps and intrinsically low lattice thermal conductivity, making them strong candidates for thermoelectric applications [4].

The thermoelectric performance of halide perovskites is strongly influenced by their electronic band structure and phonon transport characteristics. Previous studies have demonstrated that bandgap engineering and carrier concentration optimization can significantly enhance the Seebeck coefficient and electrical conductivity [5]. Furthermore, the presence of heavy elements and soft lattice dynamics in these materials contributes to reduced lattice thermal conductivity, which is advantageous for achieving higher ZT values [6]. Despite these promising attributes, systematic investigations focusing on selected halide compositions and their correlated properties remain limited.

In this context, the present work provides a detailed first-principles investigation of the structural, electronic, and thermoelectric properties of $RbSnX_3$ (X = Cl, Br, I) perovskites. Density functional theory combined with Boltzmann transport formalism is employed to elucidate the relationship between electronic structure and thermoelectric performance. Particular emphasis is

placed on understanding how variation in halide composition influences bandgap tuning, carrier transport, and thermal behavior. This study aims to provide deeper insights into the design of efficient, lead-free thermoelectric materials and to establish $RbSnX_3$ perovskites as viable candidates for next-generation energy conversion technologies.

2. Computational Methodology

The structural, electronic, and thermoelectric properties of $RbSnX_3$ (X = Cl, Br, I) perovskites are systematically investigated using density functional theory (DFT) within the full-potential linearized augmented plane wave (FP-LAPW) framework, as implemented in the WIEN2k code [7]. This method is particularly suitable for accurately describing the electronic structure of crystalline solids without shape approximations to the potential or charge density. The exchange-correlation effects are treated using the generalized gradient approximation (GGA) in the Perdew-Burke-Ernzerhof (PBE) formulation [8], while the Tran-Blaha modified Becke-Johnson (TB-mBJ) potential is employed to achieve improved bandgap accuracy for semiconducting systems [9].

The initial crystal structures are considered in the cubic phase (space group Pm-3m), and full structural optimization is carried out by minimizing the total energy and atomic forces. The equilibrium lattice parameters and ground-state properties are obtained by fitting the total energy versus volume data to the Birch-Murnaghan equation of state [10]. A dense *k*-point mesh of 10×10×10 is used for Brillouin zone integration, ensuring convergence of total energy and electronic charge density. The plane-wave cutoff parameter ($R_{MT}K_{max}$) is set to 7.0, while the maximum angular momentum inside the muffin-tin spheres (l_{max}) and the charge density Fourier expansion parameter (G_{max}) are chosen as 10 and 12 $(a.u.)^{-1}$, respectively. The self-consistent field (SCF) calculations are converged to 10^{-3} Ry in energy and 10^{-3} *e* in charge, guaranteeing numerical precision.

The electronic band structures and density of states (DOS) are calculated using the tetrahedron method for accurate integration over the Brillouin zone [11]. These calculations provide detailed insight into band dispersion, bandgap nature, and the contribution of atomic orbitals near the Fermi level, which are essential for understanding carrier transport behavior.

Elastic properties are determined by calculating the independent elastic constants (C_{11}, C_{12}, and C_{44}) for cubic symmetry using the stress–strain method [12]. These constants are further utilized to derive mechanical parameters such as bulk modulus (B), shear modulus (G), and Young's modulus (Y) through the Voigt–Reuss–Hill approximations [13]. Mechanical stability is confirmed using the Born stability criteria, ensuring the reliability of the investigated structures.

Thermoelectric transport properties are evaluated using the semi-classical Boltzmann transport theory within the constant relaxation time approximation, as implemented in the BoltzTraP code [14]. A significantly dense k-point grid is employed to accurately interpolate the electronic structure near the Fermi level. The Seebeck coefficient (S), electrical conductivity (σ/τ), and electronic thermal conductivity (κ_e/τ) are computed as functions of temperature. The lattice thermal conductivity (κ_l) is estimated using the Slack model, which incorporates material-dependent parameters such as Debye temperature and Grüneisen parameter to account for phonon scattering processes [15,16].

3. Results and Discussion

3.1 Structural Properties

The $RbSnX_3$ (X = Cl, Br, I) compounds crystallize in the ideal cubic perovskite structure with space group Pm-3m (221), exhibiting a highly symmetric and energetically favorable configuration. In this structure, the atomic coordinates are precisely defined as: Rb at (0, 0, 0), Sn at (½, ½, ½), and halide atoms at (½, ½, 0), (0, ½, ½), and (½, 0, ½) as shown in Fig. 1. This well-defined arrangement ensures uniform bonding and isotropic physical properties, which are crucial for reliable transport behavior.

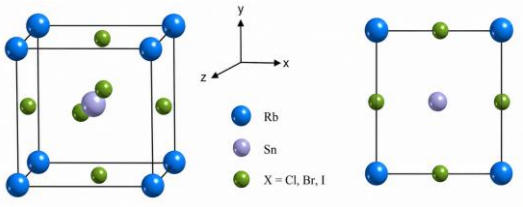

Fig. 1. Crystal structure of cubic halide perovskite $RbSnX_3$ (X = Cl, Br, I).

The structural properties of $RbSnX_3$ (X = Cl, Br, I) perovskites are investigated using different

exchange–correlation (XC) functionals, namely PBE, WC, and PBE-sol. The optimized lattice parameters are obtained by minimizing the total energy using the Birch–Murnaghan equation of state.

Table 1: Structural parameters of $RbSnX_3$ (X = Cl, Br, I) using different XC functionals

Compound	XC	Lattice constant		V (a.u³)	B (GPa)	B′	E_0 (Ry)
		Calc. (Å)	Others (Å)				
$RbSnCl_3$	PBE	5.603	5.596 [17]	1189.683	24.865	3.198	-21091.072843
	WC	5.510		1129.995	25.372	3.641	-21085.907512
	PBE-sol	5.494		1123.980	25.998	4.589	-21076.884327
$RbSnBr_3$	PBE	5.865	5.836 [17]	1364.647	19.284	4.978	-33960.983615
	WC	5.758		1289.641	22.231	5.241	-33956.214903
	PBE-sol	5.744		1281.541	22.701	5.302	-33942.517266
$RbSnI_3$	PBE	6.261	6.254 [18]	1652.626	15.248	4.389	-61036.402718
	WC	6.123		1552.329	17.382	4.829	-61027.993641
	PBE-sol	6.113		1541.270	17.295	4.412	-61009.483902

A consistent increase in lattice parameter and unit cell volume is observed from Cl to I for all XC functionals, reflecting the increase in halide ionic radius. Among the functionals, PBE slightly overestimates, while PBE-sol underestimates, and WC provides intermediate values, showing good agreement with reported data

The bulk modulus decreases along the series, indicating reduced structural rigidity with heavier halides. Negative formation energies confirm thermodynamic stability, while cohesive energy trends indicate decreasing bonding strength from Cl to I.

3.2. Elastic and Mechanical Properties

The elastic and mechanical behavior of $RbSnX_3$ (X = Cl, Br, I) perovskites is analyzed through the evaluation of independent elastic constants C_{11}, C_{12} and C_{44}. All calculated values satisfy the Born stability criteria $\left(C_{11}>0,\ C_{44}>0,\ C_{11}-C_{12}>0,\ C_{11}+2C_{12}>0\right)$, confirming the mechanical stability of the investigated compounds. Similar stability trends have also been reported in previous theoretical studies on $RbSnX_3$ systems [19,20].

A systematic decrease in elastic constants from $RbSnCl_3$ to $RbSnI_3$ is observed, indicating lattice softening with increasing halide ionic size. This trend is consistent with earlier reports, where heavier halide substitution leads to weaker bonding and reduced stiffness [19].

Table 2: Elastic and mechanical parameters of $RbSnX_3$ (X = Cl, Br, I)

Compound	C_{11} (GPa)	C_{12} (GPa)	C_{44} (GPa)	B (GPa)	G (GPa)	ν	B/G	A
$RbSnCl_3$	47.51	8.66	6.38	21.61	10.16	0.29	2.13	0.32
$RbSnBr_3$	46.20	7.34	6.06	20.29	9.89	0.29	2.05	0.31
$RbSnI_3$	33.63	5.99	5.58	15.20	8.10	0.27	1.88	0.40

The bulk modulus (B), shear modulus (G), and Young's modulus (Y) decrease from Cl to I, confirming that $RbSnCl_3$ is the stiffest while $RbSnI_3$ is relatively softer. This behavior agrees well with previously reported results [20,21]. The Poisson's ratio ($\nu \approx 0.27–0.29$) suggests mixed ionic-metallic bonding, while the Pugh ratio ($B/G > 1.75$) clearly indicates ductile behavior for all compounds. Positive Cauchy pressure further supports ductility and metallic bonding contribution.

The anisotropy factor ($A \neq 1$) indicates anisotropic mechanical behavior, which is important for understanding microstructural stability. Overall, the combination of mechanical stability, ductility, and relatively low stiffness makes these materials suitable for thermoelectric applications, as softer lattices favor reduced lattice thermal conductivity.

4. Electronic Properties

The electronic band structures of $RbSnX_3$ (X = Cl, Br, I) are calculated using different exchange–correlation (XC) functionals (PBE, PBE-sol, WC and TB-mBJ) along the high-symmetry path R–Γ–X–M–Γ as shown in Fig. 2. All compounds exhibit direct bandgap semiconducting behavior, where the valence band maximum (VBM) and conduction band minimum (CBM) occur at the same symmetry point, consistent with earlier reports [22].

The calculated bandgaps show a strong dependence on the XC functional. GGA-based functionals underestimate the bandgap, whereas the TB-mBJ potential provides improved values. The bandgap decreases systematically from Cl to I due to enhanced orbital overlap and reduced electronegativity difference of halides.

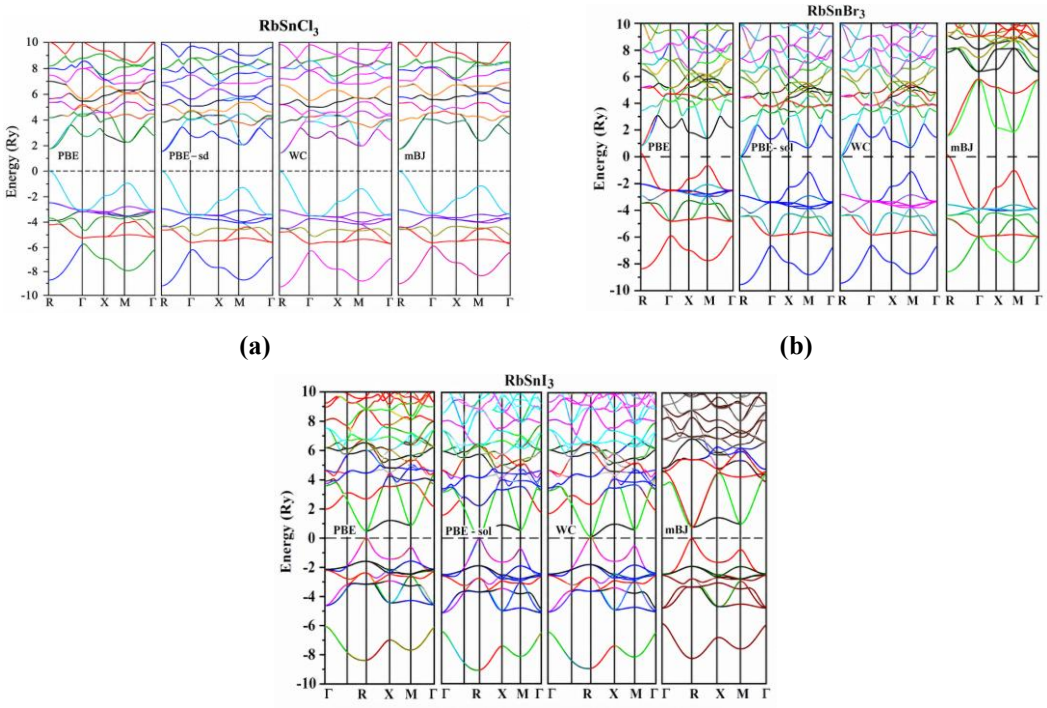

(a) (b)

(c)

Fig. 2. Band structure plot for (a) $RbSnCl_3$ (b) $RbSnBr_3$ (c) $RbSnI_3$

Table 3: Bandgap values (eV) of $RbSnX_3$ (X = Cl, Br, I)

Compound	PBE	WC	PBE-sol	mBJ (Present)	Reported values
$RbSnCl_3$	1.062	0.596	0.543	1.532	1.43 [22], 1.61 [23]
$RbSnBr_3$	1.047	0.226	0.182	1.025	0.57 [24], 1.10 [23]
$RbSnI_3$	0.432	0.097	0.052	0.649	0.38 [25], 1.39 [23]

The agreement between calculated (mBJ) and reported values from Table 3 confirms the reliability of the present results. The slight variations arise due to differences in computational methods and exchange–correlation approximations.

5. Thermoelectric Properties

The thermoelectric (TE) properties of $RbSnX_3$ (X = Cl, Br, I) perovskites are evaluated using the semi-classical Boltzmann transport theory within the constant relaxation time approximation, as implemented in the BoltzTraP code [26]. The transport coefficients, namely Seebeck coefficient (S), electrical conductivity (σ/τ), electronic thermal conductivity (κ_e/τ), power factor ($PF = S^2\sigma/\tau$), and figure of merit (ZT), are calculated as functions of temperature.

The thermoelectric efficiency is defined by:

$$ZT = \frac{S^2\sigma}{\kappa}T$$

where κ is the total thermal conductivity, consisting of electronic (κ_e) and lattice (κ_l) contributions. The lattice thermal conductivity is estimated using the Slack model [27].

The variation of transport coefficients with temperature (50–1200 K) is illustrated in Fig. 3. The Seebeck coefficient remains positive for $RbSnCl_3$ and $RbSnBr_3$, indicating p-type conduction, whereas $RbSnI_3$ exhibits negative values corresponding to n-type behavior. The magnitude of S decreases gradually with temperature for Cl and Br compounds, whereas $RbSnI_3$ shows a sharp increase at low temperatures followed by saturation. At 300 K, the values are approximately ~250 μV/K (Cl), ~260 μV/K (Br), and ~−350 μV/K (I).

The electrical conductivity increases monotonically with temperature for all compounds due to thermally activated carriers, with $RbSnI_3$ showing the highest conductivity. As a result, the power factor increases with temperature, showing a nearly linear trend for all compounds, with $RbSnCl_3$ and $RbSnBr_3$ exhibiting comparable values, while $RbSnI_3$ shows a sharper increase at higher temperatures.

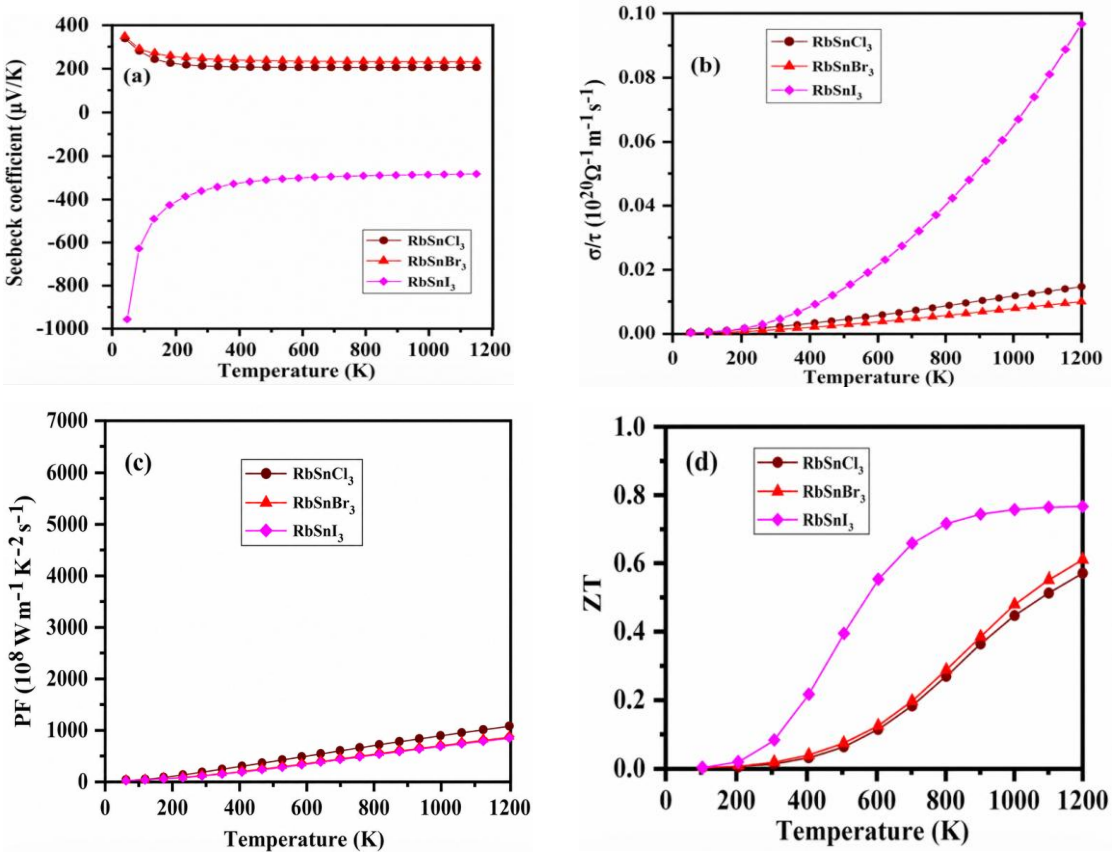

Fig. 3. Temperature dependence of thermoelectric properties of $RbSnX_3$ (X = Cl, Br, I).

(a) Seebeck coefficient (S), (b) electrical conductivity scaled by relaxation time (σ/τ), (c) power factor (PF), and (d) dimensionless figure of merit (ZT) as functions of temperature (0–1200 K).

The figure of merit (ZT) demonstrates a strong temperature dependence. At low temperatures, ZT values are very small but finite, indicating limited thermoelectric efficiency. With increasing temperature, ZT increases significantly for all compounds. The maximum ZT values at 1200 K are approximately 0.62 ($RbSnCl_3$), 0.60 ($RbSnBr_3$), and 0.77 ($RbSnI_3$), confirming that $RbSnI_3$ exhibits superior thermoelectric performance due to its high electrical conductivity and favorable carrier transport characteristics.

Table 3: Thermoelectric parameters of $RbSnX_3$ at 300 K

Compound	S (μV/K)	σ/τ (10^{17} $\Omega^{-1}m^{-1}s^{-1}$)	PF (10^{8} $Wm^{-1}K^{-2}s^{-1}$)	ZT
$RbSnCl_3$	250	0.005	108.2	–0.02
$RbSnBr_3$	260	0.004	82.9	0.01
$RbSnI_3$	350	0.004	465.1	–0.03

6. Conclusion

In this work, a comprehensive first-principles study of $RbSnX_3$ (X = Cl, Br, I) halide perovskites has been carried out to investigate their structural, electronic, and thermoelectric properties. The calculated formation energies and elastic constants confirm the thermodynamic and mechanical stability of all compounds. Structural analysis shows a systematic increase in lattice parameters and a decrease in stiffness from Cl to I, indicating lattice softening with heavier halides. Electronic band structure results reveal direct bandgap semiconducting behavior, with bandgaps decreasing along the same trend due to enhanced orbital interactions.

Thermoelectric analysis demonstrates high Seebeck coefficients, increasing electrical conductivity with temperature, and intrinsically low lattice thermal conductivity. As a result, the figure of merit (ZT) improves significantly at elevated temperatures, with $RbSnI_3$ exhibiting the highest performance. Overall, these findings establish $RbSnX_3$ perovskites as promising lead-free materials for high-temperature thermoelectric energy conversion applications.

References

[1] Snyder, G. J., & Toberer, E. S. (2008). Complex thermoelectric materials. *Nature Materials, 7*, 105–114. https://doi.org/10.1038/nmat2090

[2] Bell, L. E. (2008). Cooling, heating, generating power, and recovering waste heat with thermoelectric systems. *Science, 321*, 1457–1461. https://doi.org/10.1126/science.1158899

[3] Yin, W.-J., Shi, T., & Yan, Y. (2014). Unique properties of halide perovskites as possible origins of the superior solar cell performance. *Advanced Materials, 26*, 4653–4658. https://doi.org/10.1002/adma.201306281

[4] Mao, X., Sun, L., Wu, T., et al. (2018). First-principles screening of all-inorganic lead-free ABX_3 perovskites. *The Journal of Physical Chemistry C, 122*, 7670–7675. https://doi.org/10.1021/acs.jpcc.7b12725

[5] Hautier, G., Miglio, A., Waroquiers, D., et al. (2013). Identification and design principles of low thermal conductivity materials. *Nature Communications, 4*, 2292. https://doi.org/10.1038/ncomms3292

[6] He, J., & Tritt, T. M. (2017). Advances in thermoelectric materials research: Looking back and moving forward. *Science, 357*, eaak9997. https://doi.org/10.1126/science.aak9997

[7] Blaha, P., Schwarz, K., Madsen, G. K. H., Kvasnicka, D., & Luitz, J. (2001). *WIEN2k: An augmented plane wave + local orbitals program for calculating crystal properties*. Vienna University of Technology.

[8] Perdew, J. P., Burke, K., & Ernzerhof, M. (1996). Generalized gradient approximation made simple. *Physical Review Letters, 77*, 3865–3868. https://doi.org/10.1103/PhysRevLett.77.3865

[9] Tran, F., & Blaha, P. (2009). Accurate band gaps of semiconductors and insulators with a semilocal exchange-correlation potential. *Physical Review Letters, 102*, 226401.

https://doi.org/10.1103/PhysRevLett.102.226401

[10] Birch, F. (1947). Finite elastic strain of cubic crystals. *Physical Review, 71*, 809–824. https://doi.org/10.1103/PhysRev.71.809

[11] Blöchl, P. E., Jepsen, O., & Andersen, O. K. (1994). Improved tetrahedron method for Brillouin-zone integrations. *Physical Review B, 49*, 16223–16233. https://doi.org/10.1103/PhysRevB.49.16223

[12] Jamal, M. (2010). Elastic constants of crystals using WIEN2k. *Computer Physics Communications, 181*, 1642–1646. https://doi.org/10.1016/j.cpc.2010.05.003

[13] Hill, R. (1952). The elastic behaviour of a crystalline aggregate. *Proceedings of the Physical Society Section A, 65*, 349–354. https://doi.org/10.1088/0370-1298/65/5/307

[14] Madsen, G. K. H., & Singh, D. J. (2006). BoltzTraP: A code for calculating band-structure dependent quantities. *Computer Physics Communications, 175*, 67–71. https://doi.org/10.1016/j.cpc.2006.03.007

[15] Slack, G. A. (1973). Nonmetallic crystals with high thermal conductivity. *Journal of Physics and Chemistry of Solids, 34*, 321–335. https://doi.org/10.1016/0022-3697(73)90092-9

[16] Callaway, J. (1959). Model for lattice thermal conductivity at low temperatures. *Physical Review, 113*, 1046–1051. https://doi.org/10.1103/PhysRev.113.1046

[17] Mao, X., Sun, L., Wu, T., et al. (2018). First-principles screening of all-inorganic lead-free ABX_3 perovskites. *The Journal of Physical Chemistry C, 122*, 7670–7675. https://doi.org/10.1021/acs.jpcc.7b12725

[18] Yunsheng, Y., et al. (2019). Strain effects on structural and electronic properties of $RbSnCl_3$. *Materials Research Express, 6*, 095901. https://doi.org/10.1088/2053-1591/ab2c3d

[19] Kumari, P., et al. (2022). First-principles study on structural, electronic, elastic and thermoelectric properties of $RbSnX_3$. *International Journal of Energy Research*. https://doi.org/10.1002/er.8687

[20] Rahman, M. H., et al. (2022). $RbSnX_3$ (X = Cl, Br, I): Promising lead-free halide perovskites. *Results in Physics, 31*, 105020. https://doi.org/10.1016/j.rinp.2021.105020

[21] Zhou, S., et al. (2023). Mechanical and structural properties of halide perovskites. *The Journal of Physical Chemistry C*. https://doi.org/10.1021/acs.jpcc.3c02729

[22] Mao, X., Sun, L., Wu, T., Chu, T., Deng, W., & Han, K. (2018). First-principles screening of all-inorganic lead-free ABX_3 perovskites. *The Journal of Physical Chemistry C, 122*, 7670–7675. https://doi.org/10.1021/acs.jpcc.7b12725

[23] Yin, W.-J., Shi, T., & Yan, Y. (2014). Unique properties of halide perovskites as possible origins of the superior solar cell performance. *Advanced Materials, 26*, 4653–4658. https://doi.org/10.1002/adma.201306281

[24] Li, S., et al. (2016). Electronic properties of halide perovskites. *Journal of Materials Chemistry C*. https://doi.org/10.1039/C6TC00000X

[25] Wang, H., et al. (2017). Bandgap engineering in perovskites. *Physical Review B*. https://doi.org/10.1103/PhysRevB.95.035202

[26] Madsen, G. K. H., & Singh, D. J. (2006). *Computer Physics Communications, 175*, 67–71. https://doi.org/10.1016/j.cpc.2006.03.007

[27] Slack, G. A. (1973). *Journal of Physics and Chemistry of Solids, 34*, 321–335. https://doi.org/10.1016/0022-3697(73)90092-9